Energy & Environmental Science

PAPER

View Article Online
View Journal | View Issue

Published on 31 January 2018. Downloaded by Dalian Institute of Chemical Physics, CAS on 27/03/2018 04:34:19.

Check for updates

Cite this: *Energy Environ. Sci.*, 2018, **11**, 682

Toward a universal polymeric material for electrode buffer layers in organic and perovskite solar cells and organic light-emitting diodes†

Qiang Zhang,‡[a] Wei-Ting Wang,‡[b] Cheng-Yu Chi,[b] Tobias Wächter,[c] Jhih-Wei Chen,[d] Chou-Yi Tsai,[a] Ying-Chi Huang,[a] Michael Zharnikov, *[c] Yian Tai *[b] and Der-Jang Liaw *[a]

Received 16th November 2017,
Accepted 31st January 2018

DOI: 10.1039/c7ee03275g

rsc.li/ees

A novel concept of an electrode buffer layer material, exhibiting either hole transporting or reducing electrode work function (WF) properties, is demonstrated by the example of a polymeric compound PDTON, which can be utilized as a 'universal' electrode (either for anode or cathode) buffer layer material. Depending on the composition ratio of acetic acid and ethyl acetate upon dispersing, PDTON forms two kinds of nanospheres, serving as building blocks and defining the morphology and properties of the respective materials, termed as A-PDTON and C-PDTON. These materials are suitable for hole transport (triphenylamine on the surface of A-PDTON nanospheres) and reducing the WF of an electrode due to the formation of a suitable interfacial dipole (C-PDTON), respectively. We demonstrate the versatility and high compatibility of these two types of the same polymer in organic solar cells, organic light-emitting diodes, and perovskite solar cells, exhibiting comparable or even superior performance compared to the standard device architectures.

1. Introduction

The increasing demand for energy consumption worldwide and environmental issues trigger the development of green, renewable energy sources. These demands can be potentially met by organic photovoltaics which have achieved tremendous progress recently, having also the potential to be scaled up to make a significant impact on the overall energy mix.[1] The performance of organic photovoltaic devices relies on their building blocks. Along with the active layer, indispensable components of modern organic solar cells (OSCs)[2,3] and also organic light-emitting diodes (OLEDs)[4] are cathode and anode buffer layers (CBLs and ABLs, respectively) which have attracted great attention recently.[5–7] However, in spite of some new design concepts,[8–12] to date, most electrode buffer layer (EBL) materials suffer from complicated synthetic steps, expensive purification procedures, complex deposition techniques, and limited durability, which are not well suited for large-scale production. In particular, a typical CBL material such as lithium fluoride is a salt which can easily absorb moisture under ambient conditions, while widely used metal oxides (*e.g.* ZnO) suffer from defects and structural inhomogeneity over a large area.[13] In contrast, polymeric materials like PFN derivatives[14–17] and PEIE[18] are almost ideal compounds for CBLs due to the high efficiency of promoting electron injection and the solution-based fabrication procedure. However, the glass transition temperatures of these two kinds of materials are below 80 °C (according to the literature data[17] and our own measurements), which can hinder their application when an annealing process is required. As for the typical ABL materials, popular blends such as PEDOT:PSS are corrosive to the electrode,[19] while another frequently used ABL compound, MoO_x, is moisture sensitive.[20] Most important, each above mentioned material is only suitable for a specific type of EBL, either ABL or CBL. In addition, the parameters of these materials are mostly fixed, so that each of them is only suitable for specific device configurations, depending on particular requirements in terms of charge transport and energy level alignment. This is also true for an amphiphilic conjugated polymer serving as both ABL and CBL in OSCs developed recently.[11] With all the advantages, the performance of the OSCs using this polymer depends strongly on the electrode material and is suitable only for a few selective metals.

In the present study, however, we demonstrate a new concept of adjustment of charge transport properties in organic and

[a] *Polymer Science and Materials Lab., Department of Chemical Engineering, National Taiwan University of Science and Technology, Taipei 10607, Taiwan. E-mail: liawdj@mail.ntust.edu.tw, liawdj@gmail.com*
[b] *Nanohybrid Materials and Devices Lab., Department of Chemical Engineering, National Taiwan University of Science and Technology, Taipei 10607, Taiwan. E-mail: ytai@mail.ntust.edu.tw*
[c] *Applied Physical Chemistry, Heidelberg University, Heidelberg 69120, Germany. E-mail: Michael.Zharnikov@urz.uni-heidelberg.de*
[d] *Department of Physics, National Cheng Kung University, Tainan 70101, Taiwan*

† Electronic supplementary information (ESI) available: Experimental details and device fabrication methods. See DOI: 10.1039/c7ee03275g

‡ Q. Zhang and W.-T. Wang contributed equally to this work.

This journal is © The Royal Society of Chemistry 2018

Published on 31 January 2018. Downloaded by Dalian Institute of Chemical Physics, CAS on 27/03/2018 04:34:19.

perovskite solar cells and organic light-emitting diodes by the example of a novel, multifunctional polymeric material, PDTON, possessing tunable EBL functionalities relying on specific arrangements of the coexisting reducing electrode work function (WF, promotion of electron injection) and hole transporting groups. PDTON does not suffer from the limitations of traditional EBL materials and, what is even more important, can be selectively utilized as both CBL and ABL in organic and perovskite solar cells and organic light-emitting diodes, generalizing the concept of a bifunctional interlayer material. The main chain of PDTON consists of triphenylamine and its derivatives, which represent a hole conductor.[7] The side chains of PDTON contain aminoalkyl groups, which can reduce the WF of a substrate such as conducting polymers, metals, metal oxides, and inorganic semiconductors by generating electron transfer from the amino groups to the substrate,[18] thus forming a suitable interfacial dipole to facilitate the injection of electrons. Significantly, PDTON can be prepared in two different configurations by simply tuning the concentration of acetic acid in the dispersion solvent. Depending on this parameter, the hydrophobic polytriphenylamine chain and hydrophilic aminoalkyl pendant groups of PDTON form either A-type (for anode buffer layer) or C-type (for cathode buffer layer) nanospheres, which serve as the building blocks of the respective materials, termed as A-PDTON and C-PDTON, defining their morphology and properties. The A-PDTON nanospheres comprise the polytriphenylamine shell and the aminoalkyl core, whereas the opposite configuration occurs in the case of C-PDTON (see Fig. 1a). Significantly, the functions of A- and C-PDTON are distinctly different: A-PDTON can transport holes and works as an electron blocking layer, whereas C-PDTON generates a favourable interfacial dipole between the amino groups and electrode, modifying its WF and promoting the injection of electrons. Both types of nanospheres and, consequently, both materials can be reversibly transformed into one another, by their redispersion in a solvent of a suitable composition. Moreover, by carefully tuning the concentration of acetic acid in the solvent used to disperse PDTON, materials with intermediate properties between those of A- and C-PDTON can be formed. These materials are capable of continuously tuning the WF of an electrode, which can be used to match the energy levels at a particular interface. On this basis, as representative examples, we demonstrated the utilization of different types of PDTON as universal EBLs in OSCs, OLEDs, and perovskite solar cells (PSCs), and we obtained comparable or even superior performance of these devices compared to the standard architectures. The simplicity of tuning the EBL functionalities makes PDTON a universal EBL material for OSCs, OLEDs, and PSCs. In addition, the fully solution-based preparation procedure complies with the printing/coating processes of large-scale production.

2. Results and discussion

2.1. Structure and solubility of PDTON

The structure of PDTON is shown in Fig. 1a. Specific details related to the starting materials, synthetic routes, and characterization of the monomers and polymer can be found in the ESI.† Note

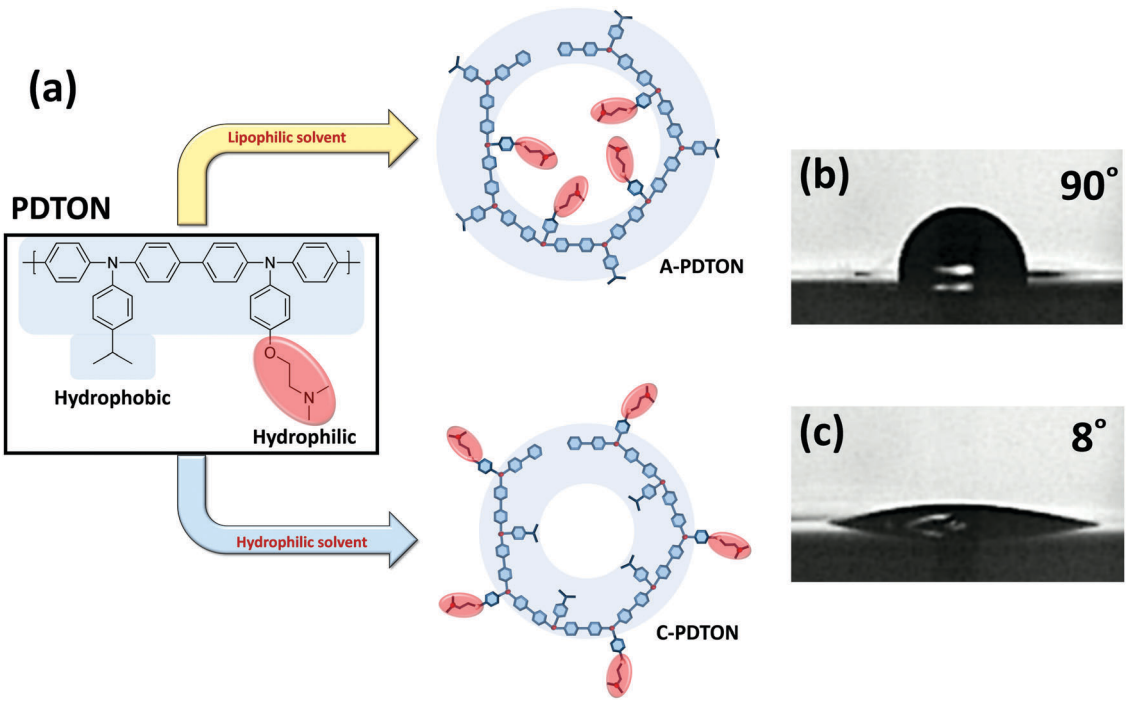

Fig. 1 Conformation of the PDTON nanospheres when aggregated. (a) Chemical structure of PDTON which possesses C- and A-PDTON morphology upon its dispersion in a proper solvent. Depending on the polarity of the solvent, two different types of nanospheres are formed, termed as A-PDTON and C-PDTON. (b) and (c) Water drops on the surface of the A-PDTON and C-PDTON films; static CAs are given, providing fingerprints for the chemical structures of the outer shell of the nanospheres.

Published on 31 January 2018. Downloaded by Dalian Institute of Chemical Physics, CAS on 27/03/2018 04:34:19.

that PDTON can be dissolved in various solvents, such as chlorobenzene and toluene. It can also be dispersed in solvents of relatively high polarity such as alcohols, water, and ethyl acetate, with addition of acetic acid. Details of the experimental procedures and information about the respective setups can be found in the Methods section.

2.2. A- and C-PDTON nanospheres

Polytriphenylamine generally shows low solubility and tends to aggregate randomly in ethyl acetate owing to its rigid backbone structure. However, upon the attachment of hydrophilic side chains to the polytriphenylamine backbone, this polymer becomes amphiphilic. It is well known that amphiphilic molecules can form micelle and inverse micelle structures in solution depending on the hydrophilicity or lipophilicity of the solvents.[21–23] In our case, PDTON was first completely dissolved in acetic acid and subsequently diluted with ethyl acetate. During this process, the aggregation state of PDTON varied depending on the concentration of acetic acid in ethyl acetate, given by the respective composition ratio, with the formation of the C- and A-PDTON nanospheres at a high and low concentration of acetic acid, respectively, as shown in Fig. 1a. The higher concentration of acetic acid in the mixed solvent results in its higher hydrophilicity[24] and *vice versa*, affecting the behavior of the hydrophilic aminoalkyl pendant groups which prefer to be exposed to a more hydrophilic solvent while polytriphenylamine shows affinity to a more lipophilic one. Accordingly, C-PDTON nanospheres with the aminoalkyl group shell and the polytriphenylamine core were formed at a high concentration of acetic acid, with a closely packed structure of triphenylamine due to the strong π–π stacking. In contrast, when the concentration of acetic acid was low, the aminoalkyl pendant groups tended to aggregate owing to the higher lipophilicity of the mixture solvent, forming the A-PDTON nanospheres. The shell of these nanospheres is composed of the polytriphenylamine backbone, whereas the core is composed of the aminoalkyl groups. Significantly, the A-PDTON film showed a static water contact angle (CA) of 90° (see Fig. 1b), whereas the C-type film exhibited a CA of only 8° (see Fig. 1c), underlining a pronounced difference between these two modifications of the same polymer. Considering that the wetting properties of the PDTON films are determined by the outer shell moieties of the nanospheres, this behavior agrees well with the proposed models in Fig. 1a, *viz.* an inward orientation of the aminoalkyl moieties (highlighted by red ovals) and an outward orientation of the polytriphenylamine main chain (highlighted by a blue ring) in A-PDTON, and the inverse orientations of these building blocks in C-PDTON. Interestingly, the solvent-induced configurations of PDTON can be reversibly changed from one type to another, by its redispersion in a suitable solvent (see Fig. S6, ESI†). This is clear evidence that no irreversible chemical changes are involved upon the formation of A- and C-PDTON, which is very important since the preparation procedure also included a post-dispersion heating up to 150–170 °C to remove the solvent and acetic acid in particular. Note, however, that the solvent removal can also be achieved at a lower temperature (100 °C), as has been demonstrated by our control experiments. This means that, if necessary, PDTON can also be used together with heat-sensitive active materials.

To confirm that there are indeed no solvent residuals and no changes in the chemical structure of PDTON upon its dispersion and subsequent heating,[25,26] nuclear magnetic resonance (NMR) measurements on the pristine PDTON as well as the A- and C-PDTON samples were carried out (Fig. S7 and S8, ESI†). The nearly identical spectra of all three samples signify the identical chemical structure albeit with insignificant variations which is entirely due to the solvent effect.

Further information is provided by near-edge X-ray absorption fine structure (NEXAFS) spectroscopy (see Fig. S9, ESI†). The C K-edge spectra of the A- and C-PDTON films prepared on ITO substrates are almost identical, as can be expected for the films of the same chemical composition – as proposed by our model. At the same time, they are very similar to the spectrum of poly[4,4′-(*N*-(4-secbutylphenyl))diphenylamine][27] which has the same backbone but a somewhat different side group (aliphatic chain) attached to the "side chain" phenyl ring. The spectra are dominated by a strong π_1^* orbital of the phenyl rings comprising the backbone and side chains of PDTON, exhibiting also a weak feature related to the C 1s (C–N) → π* transition, associated with the nitrogen atom in the backbone. Significantly, the spectra exhibit a very weak (if any at all) linear dichroism, suggesting a lack of distinct, preferable orientation of individual building blocks of PDTON, as can be expected for the proposed nanosphere structure of this material. Another important point is a lack of a π*(COOH) resonance in the spectra of both PDTON types suggesting that no residuals of acetic acid are present in the films. This resonance has a high oscillator strength and is a sensitive fingerprint feature for the presence of COOH in a sample.

In agreement with the NEXAFS data, the C 1s, N 1s, and O 1s high resolution X-ray photoelectron spectra (HRXPS) of the A- and C-PDTON films prepared on the ITO substrate are quite similar, showing no traces of COOH in the C 1s spectra (see Fig. S10, ESI†). At the same time, these spectra exhibit a dominant component peak at 284.5 eV and a weaker "shoulder" at ~286.3 eV ascribed to the polytriphenylamine backbone and the aminoalkyl-containing side chains, respectively. Significantly, the spectral weight of the side chain component is stronger for the C-PDTON films compared to the A-PDTON ones, supporting tentatively the proposed morphology of the C- and A-PDTON nanospheres. Indeed, the photoemission signal from the inner part of a nanosphere should be attenuated more strongly than that from the outer shell, so that a stronger contribution from the aminoalkyl-containing side chains can be expected in the case when they form such a shell, as proposed for C-PDTON.

Significantly, by dispersing pristine PDTON in the mixture of acetic acid and ethyl acetate at the composition ratios between those characteristic of C- and A-PDTON (55 and 15 mg ml^{-1}, respectively), PDTON materials with well-adjustable, intermediate properties could be formed. Fig. 2 summarizes the water CA values of the PDTON films fabricated from five different dispersing solutions with ratios of acetic acid and ethyl acetate of 55, 45, 35, 25, and 15 mg ml^{-1}. These films, abbreviated

 This journal is © The Royal Society of Chemistry 2018

Published on 31 January 2018. Downloaded by Dalian Institute of Chemical Physics, CAS on 27/03/2018 04:34:19.

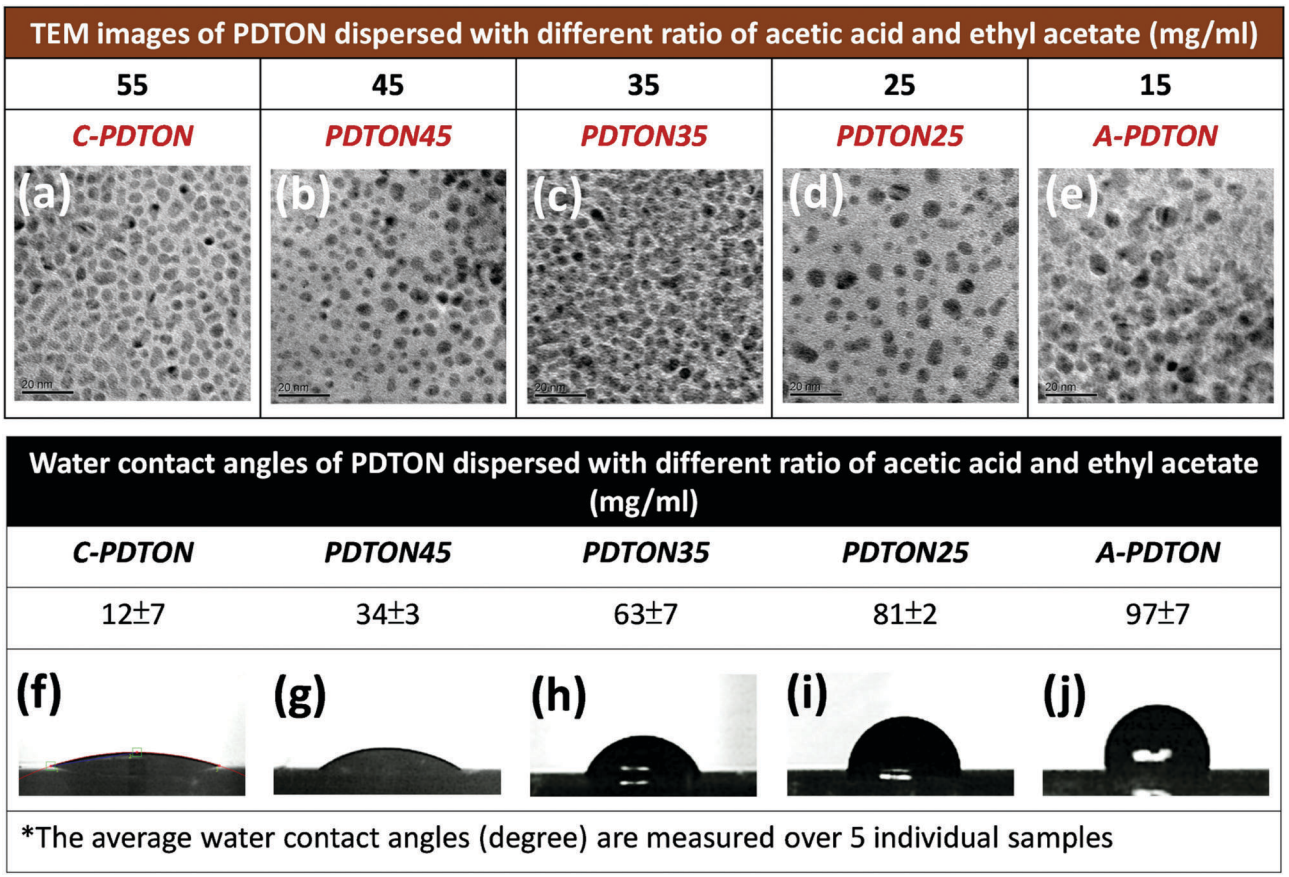

Fig. 2 HRTEM images (a–e) and static water CAs (f–j) for the PDTON films prepared from the dispersing solutions of different compositions. The ratio of acetic acid and ethyl acetate in the dispersing solution was varied across the series. The samples for the HRTEM measurements were prepared by drop-casting the diluted PDTON solutions onto carbon coated copper grids. The samples for the CA measurements were prepared by spin-casting the PDTON solutions onto the ITO substrates, followed by annealing at 150 °C for 10 min.

according to the composition ratio, showed continuously decreasing static water CAs of 97°, 81°, 63°, 34° and 12°, respectively (see Fig. 2), which we tentatively attribute to the variable portions of the A-PDTON and C-PDTON nanospheres, following the concentration of acetic acid in the solvent. As shown by atomic force microscopy (AFM), the CA behavior cannot be explained by the effect of surface roughness of the samples since it did not vary significantly along the series and the root mean square (RMS) roughness for all the films was under 10 nm (see Fig. S11, ESI†). Also, the general nanosphere morphology of these films was persistent over the series as demonstrated by the high resolution transmission electron microscopy (HRTEM) images of these five types of PDTON in Fig. 2. All these images exhibit nanospheres with a diameter of ~5 nm, which confirms our initial assumption.

2.3. HOMO–LUMO gap

The absorption onsets for both A- and C-PDTON films are located at ~440 nm (see Fig. S12a, ESI†), indicating optical bandgaps of ~2.8 eV for both types of aggregation. Electrochemical cyclic voltammograms (CVs, see Fig. S12b, ESI†) applied to both A- and C-PDTON were recorded to determine the ground-state oxidation potentials (E_{ox}), and the results indicate that the HOMO and LUMO levels of both A-PDTON and C-PDTON are located at −5.0 eV and −2.2 eV, respectively.

2.4. Hole and electron mobility

In view of applications of both configurations of PDTON in OSCs, OLEDs and PSCs, it was crucial to obtain reliable information about their electronic properties, which was achieved by the space charge limited current (SCLC) measurements. The device structures, experimental procedure, and basic equation used to derive the parameters are described in the ESI.† The log–log plots of the short-circuit current density (J_{sc}) *versus* the applied voltage (V_{app}) are presented in Fig. S13 (ESI†) and the results of the mobility evaluation are compiled in Table 1; the hole and electron mobilities of the A-PDTON films were estimated to be 5.90×10^{-4} cm^2 V^{-1} s^{-1} and 1.70×10^{-5} cm^2 V^{-1} s^{-1}, respectively. On the other hand, the analogous values for the C-PDTON films were 8.90×10^{-6} cm^2 V^{-1} s^{-1} and 1.28×10^{-5} cm^2 V^{-1} s^{-1}, respectively. In the case of A-PDTON, the electron mobility is more than one order of magnitude lower than the hole mobility which is associated with the specific structure of its nanospheres: whereas the holes can be easily transported through the polytriphenylamine main chain forming the outer shell of the nanospheres, or hop

Published on 31 January 2018. Downloaded by Dalian Institute of Chemical Physics, CAS on 27/03/2018 04:34:19.

Table 1 Hole and electron mobility of the A- and C-PDTON films derived from the SCLC data

Type	μ_h ($cm^2\ V^{-1}\ s^{-1}$) ITO/PEDOT:PSS/PDTON/PEDOT:PSS/Ag	μ_e ($cm^2\ V^{-1}\ s^{-1}$) ITO/ZnO/PDTON/ZnO/Al
A-Type	5.90×10^{-4}	1.70×10^{-5}
C-Type	8.90×10^{-6}	1.28×10^{-5}

between them, electron injection is difficult due to a large barrier associated with the wide bandgap. In contrast, for C-PDTON, the polytriphenylamine main chain is surrounded by the aminoalkyl groups which are capable of trapping most of the holes, resulting in a decrease in the hole mobility to $8.90 \times 10^{-6}\ cm^2\ V^{-1}\ s^{-1}$ and qualifying C-PDTON as a good hole blocking material. At the same time, since the polar aminoalkyl groups in the polymer film have low conductivity, the electron transfer through the main chain becomes more difficult and the electron mobility drops to $1.28 \times 10^{-5}\ cm^2\ V^{-1}\ s^{-1}$. Based on the above analysis, it can thus be concluded that A-PDTON possesses higher mobility of holes as compared to electrons, which qualifies it as an ABL. In contrast the C-PDTON film has somewhat higher electron than hole mobility, with comparably low values of these parameters. However, the interfacial dipole formed by the aminoalkyl groups when they come into contact with an electrode is capable of reducing the WF of this electrode, promoting the injection of electrons, which qualifies C-PDTON as a CBL. These properties are the basis for the use of the A- and C-PDTON films as EBLs in OSCs, OLEDs and PSCs.

2.5. Work function

The WF of the ITO surface modified with A- and C-PDTON was measured by ultraviolet photoelectron spectroscopy (UPS) and the results are compiled in Table 2. A-PDTON/ITO exhibited a comparably high WF of 4.96 eV, which is close to that of pristine ITO. This result is expected because the shell of A-PDTON is composed of polytriarylamine, which does not modify the WF of ITO. On the other hand, the WF of C-PDTON/ITO was 4.27 eV, which is by 0.7 eV lower than that of pristine ITO. This behavior suggests that the aminoalkyl groups of C-PDTON promote the charge injection and signifies the qualification of C-PDTON as a CBL, since the most important property of a CBL is the ability to modify the cathode WF in order to reduce the electron injection barrier. Notably, the interfacial dipole provided by C-PDTON stems from the electron transfer from the amino groups to the adjacent electrode,[18] which is different from the polyelectrolyte dipole generated by anionic or cationic molecules covalently bonded to the main chain and their counterions.

Table 2 Work function values (eV) of PDTON-coated ITO. The ratio of acetic acid and ethyl acetate in the dispersing solution was varied across the series

C-PDTON[a]	PDTON45[a]	PDTON35[a]	PDTON25[a]	A-PDTON[a]
4.27 ± 0.07	4.51 ± 0.04	4.70 ± 0.02	4.85 ± 0.07	4.96 ± 0.02

[a] The values were averaged over 5 individual samples.

Beyond the ultimate WF values for A- and C-PDTON coated ITO, the work function of this substrate could be continuously varied by changing the composition of the dispersing solution between those characteristic of A- and C-PDTON. The results are compiled in Table 2 and visualized in Fig. S14 (ESI†). Note that the UPS-derived WF values were additionally verified by complementary Kelvin probe measurements (see Fig. S15, ESI†), with good agreement between the results.

2.6. Device configurations

To demonstrate the reliability and versatility of the A- and C-PDTON films as EBLs in OSCs, OLEDs, and PSCs, they were tested in various device configurations as described below. Also, a PDTON film with intermediate properties was tested in a specific configuration, as a representative example.

2.7. Organic solar cells

The C- and A-PDTON films were assembled in OSCs with the general configuration of ITO/ZnO/P3HT:$PC_{61}BM$/MoO_x/Ag, substituting the electron (ZnO) and hole (MoO_x) transporting layers, respectively. The structures, energy level alignment diagrams, and the basic (J–V) characteristics of the resulting devices, *viz.* ITO/C-PDTON/P3HT:$PC_{61}BM$/MoO_x/Ag, ITO/ZnO/P3HT:$PC_{61}BM$/A-PDTON/Ag, and ITO/C-PDTON/P3HT:$PC_{61}BM$/A-PDTON/Ag, abbreviated as CBLD, ABLD, and CABLD, respectively, are shown in Fig. 3 and Fig. S16 (ESI†). The most important parameters of these assemblies, including J_{sc}, open circuit voltage (V_{oc}), fill factor (FF), and power conversion efficiency (PCE), are compiled in Table S1 (ESI†). For the preparation of CBLD, C-PDTON (10 nm) was spin-coated onto the ITO substrate; for the preparation of ABLD, A-PDTON (20 nm) was deposited on top of P3HT:$PC_{61}BM$. Fig. S16b (ESI†) shows the energy level alignment diagram for the OSC assembly utilizing PDTON as both CBL and ABL, relevant also for the ABLD and CBLD configurations. The high LUMO of A-PDTON makes it an efficient electron blocking layer, while its suitable HOMO level (−5.0 eV) facilitates the hole transport by reducing the hole injection barrier to the Ag electrode. At the same time, C-PDTON lowers the WF of the ITO electrode, promoting the injection of electrons. Accordingly, the performance of the CBLD and ABLD devices, where either CBL or ABL was substituted by the suitable form of PDTON, is comparable or even better than that of the standard device, ITO/ZnO/P3HT:$PC_{61}BM$/MoO_x/Ag, in terms of J_{sc}, FF, and PCE (see Fig. S16 and Table S1, ESI†) as well as external quantum efficiency (EQE) (see Fig. S17, ESI†). Also, the CABLD assembly, where both CBL and ABL were substituted by PDTON, exhibited a performance comparable to that of the standard device, as shown in Fig. 3c and d, where the J–V characteristics and EQE of CABLD are presented (see also Table S1, ESI†). These data confirm that the PDTON can efficiently serve as either CBL or ABL (or both of them), depending on the polymer configuration (C- or A-PDTON).

 This journal is © The Royal Society of Chemistry 2018

Published on 31 January 2018. Downloaded by Dalian Institute of Chemical Physics, CAS on 27/03/2018 04:34:19.

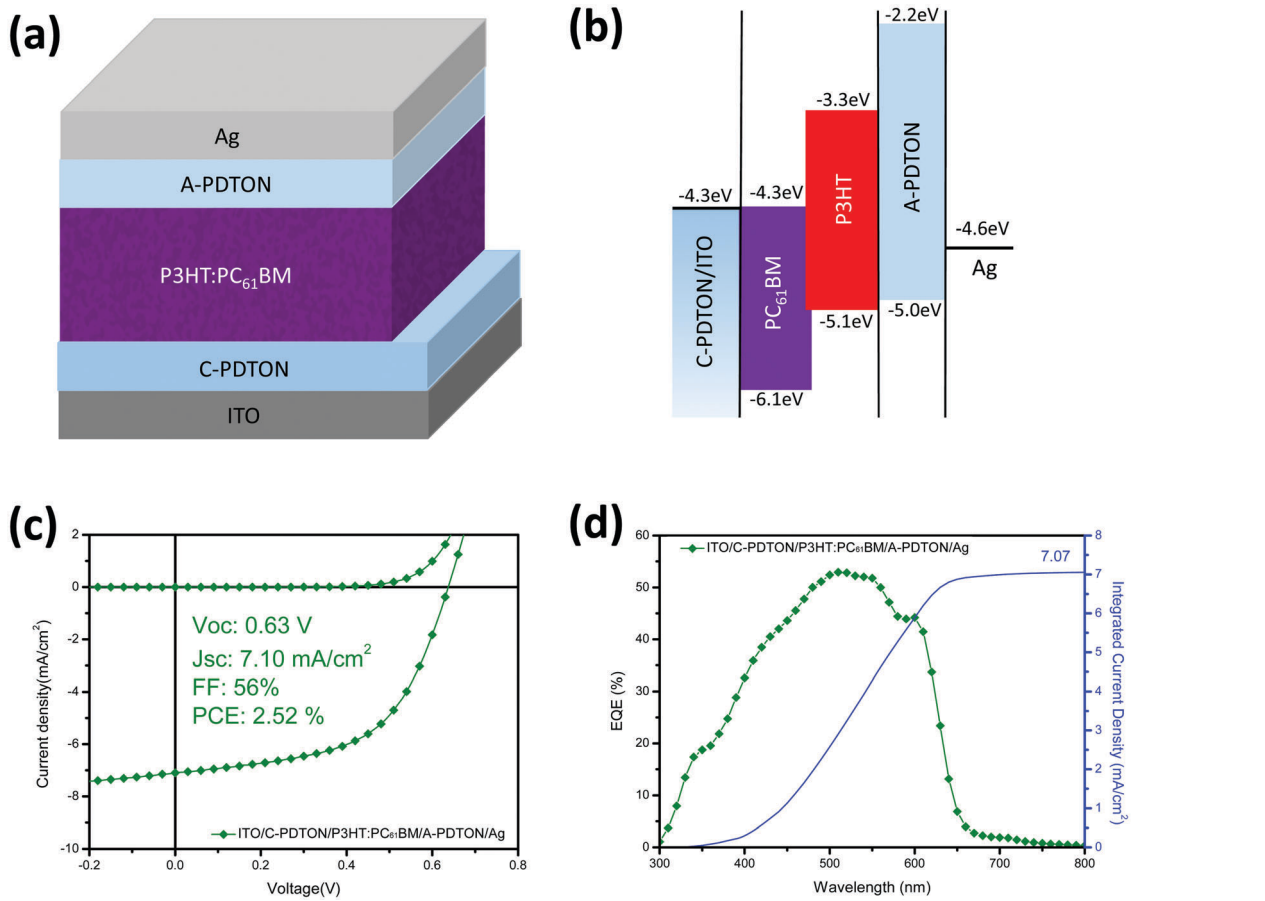

Fig. 3 Structure, energy level alignment diagram, and basic characteristics of a model OSC (CABLD). (a) Schematic of the device, in which P3HT:$PC_{61}BM$ is sandwiched between the C-PDTON and A-PDTON EBLs. (b) Energy level alignment diagram of the given OSC under the flat band conditions. (c) *J*–*V* characteristics of the given OSC under 100 mW cm^{-2} AM 1.5G illumination. (d) EQE and integrated J_{sc} of the OSC. The integrated current density calculated from EQE was 7.07 mA cm^{-2}, in good agreement with the results of the *J*–*V* measurements.

2.8. Organic light-emitting diodes

The C- and A-PDTON films were also used as the CBL and ABL of model OLEDs, respectively. Four different devices were assembled, all employing blue-light-emitting polyfluorene (PFO) as the light emitting layer. The structures of these devices are shown in Fig. 4a and b, and Fig. S19 (ESI†). For their fabrication, all layers except for the Al electrode were spin-coated. For the device configurations in Fig. 4b as well as in Fig. S19c and d (ESI†, the same configuration as in Fig. 4b), a very thin layer of PEDOT:PSS was used for separating the A-PDTON film and the PFO layer because A-PDTON would dissolve in chloroform used as the solvent for the fabrication of the PFO layer.

The modification of the Al cathode of the standard device (Fig. 4a and Fig. S19a, ESI†) with C-PDTON (see Fig. S19b, ESI†) resulted in an increase of the external efficiency (η_{ext}) from 0.02 Cd A^{-1} to 0.11 Cd A^{-1} at 10.0 V and an improvement of luminance from below 4 Cd m^{-2} to 100 Cd m^{-2} (see Fig. S19e, ESI†). This improvement can be only explained by the formation of a suitable interfacial dipole, suggesting that C-PDTON reduced the WF of Al, facilitating electron injection from the cathode. Alternatively, the modification of the ITO anode of the standard device with A-PDTON (see Fig. S19c, ESI†) also resulted in an improvement of its performance (see Fig. S19e and f, ESI†). Finally, even larger improvement was achieved upon the use of the PDTON films as both ABL and CBL (see Fig. 4b and Fig. S19d, ESI†). According to the characteristics of such a device (Fig. 4c and d), the onset of the light emission decreased from 8.2 V to 4.1 V. In addition, an average light output of 289 Cd m^{-2} was achieved with a η_{ext} = 0.24 Cd A^{-1} at a low voltage (~6 V), relying on the electron blocking ability of A-PDTON.[28] The above light output is comparable to the values reported for PFO-based OLEDs in the literature[14,29,30] and is three times higher than that of the device utilizing only C-PDTON(as CBL; see Fig. S19b, ESI†). Accordingly, the additional use of the A-PDTON film as the ABL significantly improves the OLED performance. Also, the 100 Cd m^{-2} luminance could be obtained at 4.9 V for the ITO/A-PDTON/PEDOT:PSS/PFO/C-PDTON/Al device (Fig. 4b and see Fig. S19d, ESI†), whereas the analogous luminance for the ITO/PEDOT:PSS/PFO/C-PDTON/Al device (see Fig. S19b, ESI†) could be only obtained at 10 V. We also fabricated a device without the PEDOT-PSS interlayer (ITO/A-PDTON/PFO/C-PDTON/Al), with a similar luminescence to that with the interlayer (ITO/PEDOT:PSS/PFO/C-PDTON/Al). This confirms the effectiveness of A-PDTON and C-PDTON as EBLs (see Fig. S20, ESI†).

Published on 31 January 2018. Downloaded by Dalian Institute of Chemical Physics, CAS on 27/03/2018 04:34:19.

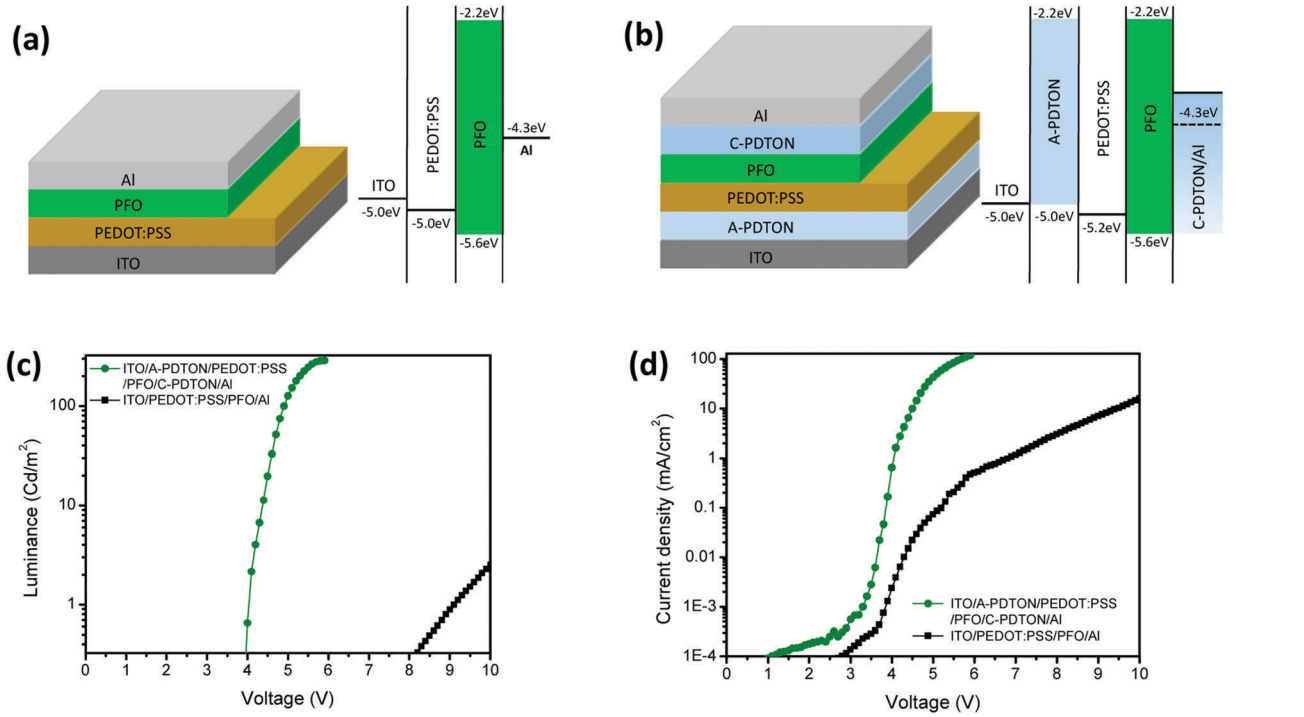

Fig. 4 Structures, energy level alignment diagrams, and characteristics of model OLEDs. (a) Schematic of a standard OLED, in which PFO is sandwiched between the PEDOT:PSS and Al layers, along with the respective energy level alignment diagram. (b) Schematic of the modified OLED, with A-PDTON and C-PDTON serving as the ABL and CBL, respectively, along with the respective energy level alignment diagram. (c) and (d) The luminance *versus* voltage and current density *versus* voltage plots for the devices (a) and (b).

2.9. Perovskite solar cells

To further illustrate the performance and versatility of PDTON, serving, depending on the type, as either ABL or CBL, conventional and inverted PSCs employing PDTON buffer layers were fabricated. These devices were assembled under ambient conditions (except the top electrode) at a relative humidity of ~55% and a temperature of 25 °C. Fig. 5a, b, d, e, g and h show the respective configurations, *viz.* those of the standard devices (see Fig. 5a, d and g), CBL-substituted devices (CBLD; see Fig. 5b and e), and ABL substituted device (ABLD; see Fig. 5h). The CBLD configuration was realized for both ZnO and SnO_2 CBLs (see Fig. 5b and e) with the C-PDTON and PDTON35 buffer layers, respectively, matching the work function of ZnO (4.3 eV)[31] and SnO_2 (4.7–4.8 eV).[32] This example demonstrates the tunability of PDTON in terms of energy level alignment in a specific device, relying on the precise adjustment of the WF by setting the concentration of acetic acid in the dispersing solution (Table 2). The device using C-PDTON/ZnO (PCE of 15.96%) exhibited higher J_{sc} (21.10 mA cm^{-2}) and FF (73.26%) than the standard device (J_{sc}: 17.81 mA cm^{-2}, FF: 69.08%, PCE: 12.51%) using only ZnO (see Fig. 5c). Also the device using PDTON35/SnO_2 (PCE of 17.06%) exhibited higher J_{sc} (21.03 mA cm^{-2}) and FF (76.39%) than the standard device (J_{sc}: 20.03 mA cm^{-2}, FF: 71.53%, PCE: 15.16%) using only SnO_2 (see Fig. 5f). In both cases, the observed enhancement of J_{sc} and FF stems presumably from the suitable interfacial dipoles provided by the PDTON films improving the electron extraction. In addition, these films served as a hole blocking layer in the given device configurations.

In the ABLD configuration of the inverted device (Fig. 5h), the A-PDTON replaced the PEDOT:PSS film (Fig. 5g), serving as both hole transporting and electron blocking layer. The PCE of the modified device (8.90%) was higher than that of the device using PEDOT:PSS as the ABL (7.40%, comparable to the performance of the device assembled using two-step deposition of a fully ambient-processed perovskite[33]).

The most important parameters of the model PSCs, including J_{sc}, V_{oc}, FF, and PCE, are compiled in Table S2 (ESI†). Note that in addition to the favorable EBL functionalities, PDTON films promote the growth of high quality perovskite overlayers. The EQE data and the integrated current density of the conventional and inverted cells are shown in Fig. S21 (ESI†), being in agreement with the current density values obtained from the *J–V* measurements. The results of the complementary X-ray diffraction (XRD) experiments are shown in Fig. S22 (ESI†). Benefiting from the surface hydrophobicity,[34] the perovskite film grown on the A-PDTON substrate exhibited higher intensity of the (110) peak than that on the PEDOT:PSS substrate, resulting, consequently, in the higher V_{oc} of the A-PDTON PSC as compared to the PEDOT:PSS device.[34,35]

2.10. Mechanism and stability

The C- and A-PDTON nanospheres, serving as building blocks of the respective polymeric materials and playing the major role in their properties, could be directly visualized by HRTEM, while the inner organization of these nanospheres, proposed by us, follows the general logic of the behavior of amphiphilic

 This journal is © The Royal Society of Chemistry 2018

Published on 31 January 2018. Downloaded by Dalian Institute of Chemical Physics, CAS on 27/03/2018 04:34:19.

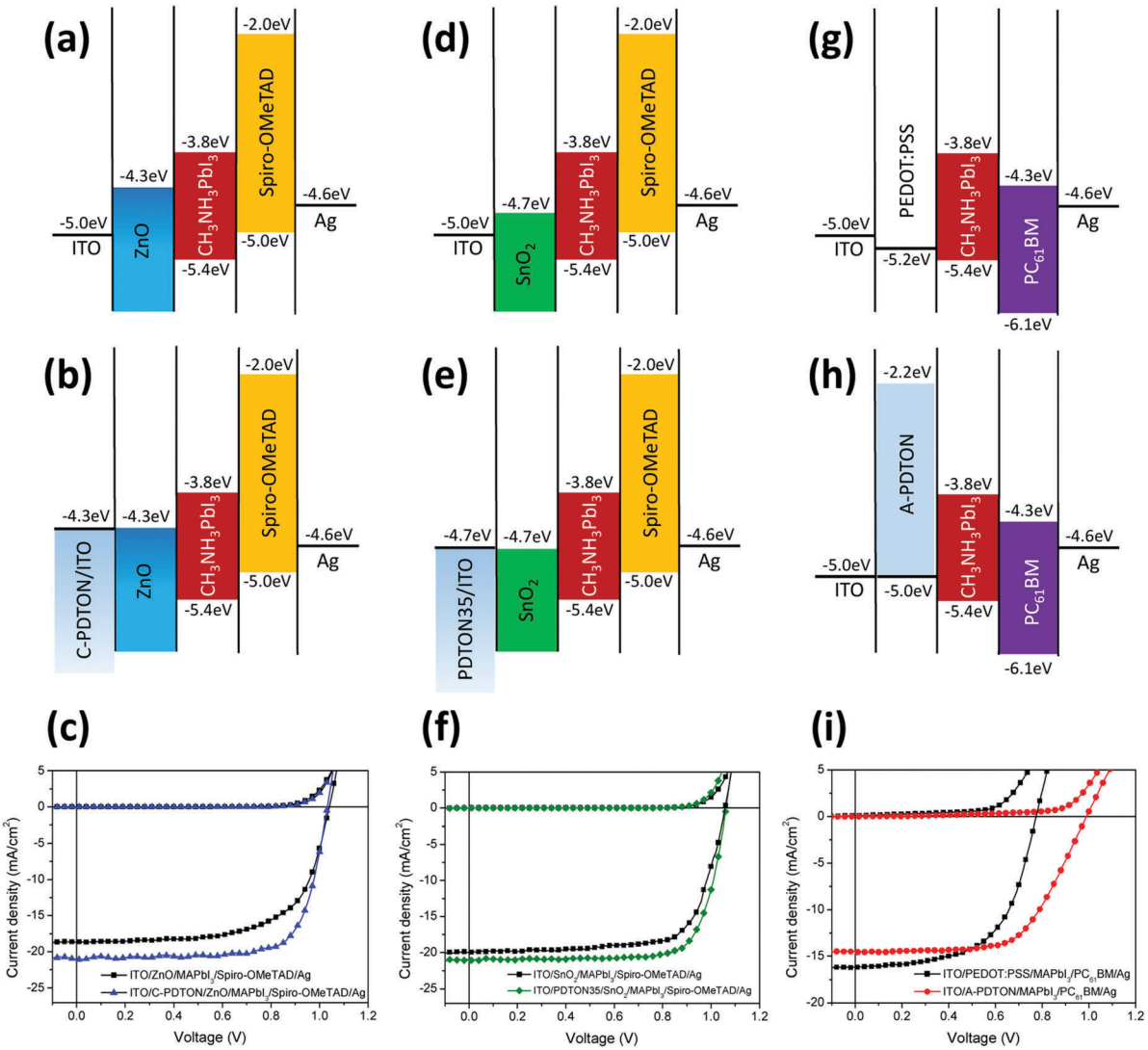

Fig. 5 Energy level alignment diagrams and basic characteristics of model PSCs. Schematics and energy level alignment diagrams of conventional and inverted PSCs, employing (a) ZnO or (b) C-PDTON/ZnO films as CBL, (d) SnO_2 or (e) PDTON35/SnO_2 films as the CBL, and (g) PEDOT:PSS or (h) A-PDTON films as the ABL. The *J*–*V* characteristics of (c) (black squares: ITO/ZnO/$CH_3NH_3PbI_3$/Spiro-OMeTAD/Ag; blue triangles: ITO/C-PDTON/ZnO/$CH_3NH_3PbI_3$/Spiro-OMeTAD/Ag), the conventional PSC using ZnO (a) and (b), (f) (black squares: ITO/SnO_2/$CH_3NH_3PbI_3$/Spiro-OMeTAD/Ag; green squares: ITO/PDTON35/SnO_2/$CH_3NH_3PbI_3$/Spiro-OMeTAD/Ag), the conventional PSC using SnO_2 (d) and (e), and (i) (black squares: ITO/PEDOT:PSS/$CH_3NH_3PbI_3$/PC_{61}BM/Ag; red dots: ITO/A-PDTON/$CH_3NH_3PbI_3$/PC_{61}BM/Ag), the inverted PSCs (g and h) under 100 mW cm^{-2} AM 1.5G illumination.

molecules in solutions with a specific concentration of acetic acid.[21–23] The indirect evidence for the structure of the C- and A-PDTON nanospheres upon going from A- to C-PDTON was provided by the CA and XPS data. Possible effects of molecular doping and irreversible chemical changes upon the formation of A- and C-PDTON could be excluded based on the NMR, HRXPS, and NEXAFS spectroscopy results.

A presumable charge transfer mechanism in the A- and C-PDTON films is schematically illustrated in Fig. 6, based on the well-studied OSC configuration, employing P3HT:PC_{61}BM as the active layer. The charge separation occurs in the active layer, and the holes and electrons are transferred to the electrodes through the A- and C-PDTON interlayers, depending on their EBL functionalities. For the A-PDTON films, the holes should be predominantly localized within the polytriphenylamine main chain, hopping efficiently along this moiety and between the nanospheres. At the same time, because this main chain possesses a high LUMO level of approximately −2.2 eV, which effectively blocks the electrons, their injection and transfer through A-PDTON would be not efficient. According to the results of the SCLC measurements, the hole mobility of the A-PDTON films (5.90×10^{-4} cm^2 V^{-1} s^{-1}) is considerably higher than their electron mobility (1.70×10^{-5} cm^2 V^{-1} s^{-1}), qualifying these films as potential ABLs, which was verified in the given study by the experiments on the model OSC, OLED, and PSC devices. In contrast, for the C-PDTON films, the inverse arrangement of the polytriphenylamine main chains and aminoalkyl groups takes place (Fig. 6, at the right). This results in the appearance of an interfacial dipole, formed between the amino groups and the adjacent electrode,[18] which

Published on 31 January 2018. Downloaded by Dalian Institute of Chemical Physics, CAS on 27/03/2018 04:34:19.

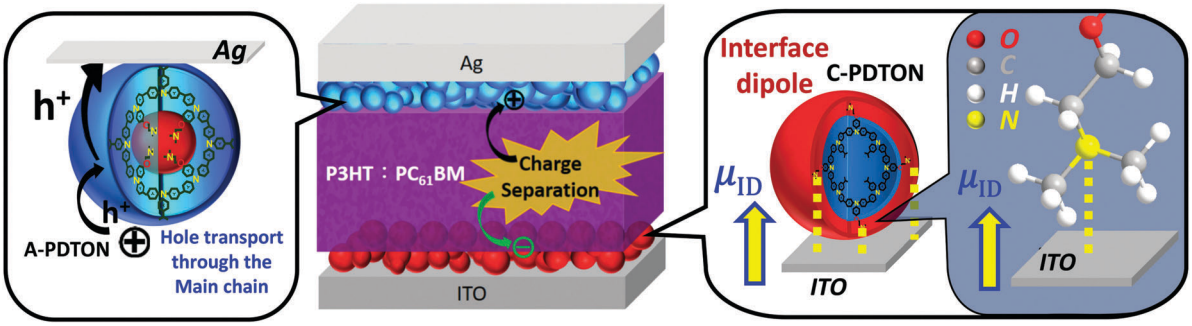

Fig. 6 Schematic of the charge carrier transfer and electron injection promotion in an OSC employing the PDTON layers. Hole transport in A-PDTON: the holes are transferred along the polytriphenylamine main chain and hop between individual nanospheres. Electron injection promoted by C-PDTON: the C-PDTON layer is inserted between the active layer and the ITO cathode; aminoalkyl side chains provide a suitable interfacial dipole lowering the height of the injection barrier for electrons.

reduces the WF of the electrode and facilitates the injection of electrons, qualifying these films as potential CBLs. Moreover, by varying the ratio of acetic acid and ethyl acetate in the dispersing solution between the values characteristic of A- and C-PDTON, PDTON layers with intermediate characteristics can be prepared. Accordingly, the WF of these layers can be precisely tuned to match the energy levels at a particular interface in a specific device, as was demonstrated by the example of a PSC employing such a layer.

An important issue in the context of device fabrication is the stability of A-PDTON and C-PDTON. The stability of the respective A-PDTON and C-PDTON nanospheres under different conditions, including the ambient (55% relative humidity and 25 °C), glove box (0% relative humidity and 25 °C) and harsh conditions (85% relative humidity and 85 °C), was monitored by HRTEM (Fig. S23c, ESI†). Even under the harsh conditions no visible degradation of the PDTON nanospheres has been observed within the time frame of our experiment (5 days) (Fig. S23c, ESI†).

3. Conclusions

In this work, we demonstrate a novel concept in context of OSC, OLED and PSC fabrication by developing a universal EBL polymer, PDTON, which possesses hole transporting properties and reduces the WF of electrodes. These coexisting functionalities rely on the specific morphology of PDTON consisting of nanospheres with specific organization (two types) defined by the mixing ratio of acetic acid and ethyl acetate in a mixed solution used for dispersing the original PDTON polymer. By casting from the respective solutions, two types of films comprising the same material but possessing distinctly different EBL functionalities could be prepared. One of these films could be used as an ABL and the other as a CBL in the model OSCs, OLEDs, and PSCs, resulting in a comparable or even superior performance compared to the standard, reference devices. In addition, we demonstrated that the properties of PDTON can be varied continuously between the ultimate cases of A- and C-PDTON by precise adjustment of the ratio of acetic acid and ethyl acetate in the dispersing solution. Among other options, this allows a precise tuning of work functions of cathodes with a single CBL material as was demonstrated for a model PSC.

Author contributions

Q. Zhang synthesized the polymers. W.-T. Wang fabricated the PSCs. Q. Zhang and W.-T. Wang measured the properties of the polymer, fabricated and measured the properties of the OSC and OLED devices, and wrote some parts of the manuscript. C.-Y. Chi assisted the fabrication of the OSC devices. W.-T. Wang and J.-W. Chen performed the UPS measurements. C.-Y. Tsai helped to synthesize the monomer and proofread the manuscript. Y.-C. Huang assisted the synthesis of PDTON. T. Wächter and M. Zharnikov performed the XPS, NEXAFS spectroscopy, and Kelvin probe measurements. Y. Tai designed the concept, supervised the experiments, and interpreted the data. Y. Tai and D.-J. Liaw supervised the entire project. Y. Tai and M. Zharnikov compiled and finalized the manuscript.

Conflicts of interest

There are no conflicts to declare.

Acknowledgements

We recognize the financial support of the Ministry of Science and Technology (MOST 105-2221-E-011-153) and (MOST 103-2628-M-011-001-MY3) including MOST-DAAD PPP travel grant (MOST 104-2911-I-011-504-MY2) which was also partly funded by DAAD. We also recognize the financial support of the Deutscher Akademischer Austauschdienst (project number 57138310). T. Wächter and M. Zharnikov thank Helmholtz Zentrum Berlin (HZB) for the allocation of synchrotron radiation beamtime and A. Nefedov and Ch. Wöll (KIT) for technical cooperation at BESSY II (HZB). Q. Zhang, W.-T. Wang and Y. Tai are grateful to C.-H. Chen (NSSRC) and C.-L. Wu (NCKU) for the technical support of UPS measurements. We are thankful to P.-T. Chou and Y.-Y. Yang (NTU) for help with HRTEM measurements. We are also thankful to Prof. S.-M. Chang (NTUT) and Prof. S. S. Yap (MMU) for the valuable comments of OLED.

 This journal is © The Royal Society of Chemistry 2018

Published on 31 January 2018. Downloaded by Dalian Institute of Chemical Physics, CAS on 27/03/2018 04:34:19.

Notes and references

1 S. B. Darling and F. You, *RSC Adv.*, 2013, **3**, 17633–17648.
2 M. M. Lee, J. Teuscher, T. Miyasaka, T. N. Murakami and H. J. Snaith, *Science*, 2012, **338**, 643–647.
3 M. Liu, M. B. Johnston and H. J. Snaith, *Nature*, 2013, **501**, 395–398.
4 J. H. Burroughes, D. D. C. Bradley, A. R. Brown, R. N. Marks, K. Mackay, R. H. Friend, P. L. Burns and A. B. Holmes, *Nature*, 1990, **347**, 539–541.
5 H. Y. Chen, J. Hou, S. Zhang, Y. Liang, G. Yang, Y. Yang, L. Yu, Y. Wu and G. Li, *Nat. Photonics*, 2009, **3**, 649–653.
6 R. H. Friend, R. W. Gymer, A. B. Holmes, J. H. Burroughes, R. N. Marks, C. Taliani, D. D. C. Bradley, D. A. Dos Santos, J. L. Brédas, M. Lögdlund and W. R. Salaneck, *Nature*, 1999, **397**, 121–128.
7 Q. D. Ling, D. J. Liaw, C. Zhu, D. S. H. Chan, E. T. Kang and K. G. Neoh, *Prog. Polym. Sci.*, 2008, **33**, 917–978.
8 N. Chakravarthi, K. Gunasekar, W. Cho, D. X. Long, Y.-H. Kim, C. E. Song, J.-C. Lee, A. Facchetti, M. Song, Y.-Y. Noh and S.-H. Jin, *Energy Environ. Sci.*, 2016, **9**, 2595–2602.
9 B. H. Lee, J. H. Lee, S. Y. Jeong, S. B. Park, S. H. Lee and K. Lee, *Adv. Energy Mater.*, 2015, **5**, 1401653.
10 C. G. Tang, M. C. Y. Ang, K. K. Choo, V. Keerthi, J. K. Tan, M. N. Syafiqah, T. Kugler, J. H. Burroughes, R. Q. Png, L. L. Chua and P. K. H. Ho, *Nature*, 2016, **539**, 536–541.
11 B. Xu, Z. Zheng, K. Zhao and J. Hou, *Adv. Mater.*, 2016, **28**, 434–439.
12 Y.-C. Tseng, A. U. Mane, J. W. Elam and S. B. Darling, *Sol. Energy Mater. Sol. Cells*, 2012, **99**, 235–239.
13 C. E. Small, S. Chen, J. Subbiah, C. M. Amb, S. W. Tsang, T. H. Lai, J. R. Reynolds and F. So, *Nat. Photonics*, 2012, **6**, 115–120.
14 H. Wu, F. Huang, Y. Mo, W. Yang, D. Wang, J. Peng and Y. Cao, *Adv. Mater.*, 2004, **16**, 1826–1830.
15 Z. He, C. i. Zhong, S. Su, M. Xu, H. Wu and Y. Cao, *Nat. Photonics*, 2012, **6**, 591–595.
16 Z. He, B. Xiao, F. Liu, H. Wu, Y. Yang, S. Xiao, C. Wang, T. P. Russell and Y. Cao, *Nat. Photonics*, 2015, **9**, 174–179.
17 K. Zhang, C. Zhong, S. Liu, C. Mu, Z. Li, H. Yan, F. Huang and Y. Cao, *ACS Appl. Mater. Interfaces*, 2014, **6**, 10429–10435.
18 Y. Zhou, C. F. Hernandez, J. Shim, J. Meyer, A. J. Giordano, H. Li, P. Winget, T. Papadopoulos, H. Cheun, J. Kim, M. Fenoll, A. Dindar, W. Haske, E. Najafabadi, T. M. Khan, H. Sojoudi, S. Barlow, S. Graham, J. L. Brédas, S. R. Marder, A. Kahn and B. Kippelen, *Science*, 2012, **336**, 327–332.
19 K. H. Ok, J. Kim, S. R. Park, Y. Kim, C. J. Lee, S. J. Hong, M. G. Kwak, N. Kim, C. J. Han and J. W. Kim, *Sci. Rep.*, 2015, **5**, 9464.
20 E. S. R. Bovill, J. Griffin, T. Wang, J. W. Kingsley, H. Yi, A. Iraqi, A. R. Buckley and D. G. Lidzey, *Appl. Phys. Lett.*, 2013, **102**, 183303.
21 J. N. Israelachvili, *Intermolecular and surface forces*, Academic Press, Boston, 1992.
22 D. Beattie, K. H. Wong, C. Williams, L. A. P. Warren, T. P. Davis, C. B. Kowollik and M. H. Stenzel, *Biomacromolecules*, 2006, **7**, 1072–1082.
23 T. S. Kale, A. Klaikherd, B. Popere and S. Thayumanavan, *Langmuir*, 2009, **25**, 9660–9670.
24 C. Reichardt and T. Welton, *Solvents and solvent effects in organic chemistry*, Wiley-VCH Verlag GmbH & Co. KGaA, 2010.
25 B. Liu, W. L. Yu, Y. H. Lai and W. Huang, *Macromolecules*, 2002, **35**, 4975–4982.
26 H. S. Van Klooster and W. A. Douglas, *J. Phys. Chem.*, 1945, **49**, 67–70.
27 B. Watts, S. Swaraj, D. Nordlund, J. Lüning and H. Ade, *J. Chem. Phys.*, 2011, **134**, 024702.
28 H. Yan, B. J. Scott, Q. Huang and T. J. Marks, *Adv. Mater.*, 2004, **16**, 1948–1953.
29 M. Gross, D. C. Müller, H. G. Nothofer, U. Scherf, D. Neher, C. Bräuchle and K. Meerholz, *Nature*, 2000, **405**, 661–665.
30 G. Latini, L. W. Tan, F. Cacialli and S. R. P. Silva, *Org. Electron.*, 2012, **13**, 992–998.
31 S. Nam, J. Seo, S. Woo, W. H. Kim, H. Kim, D. D. C. Bradley and Y. Kim, *Nat. Commun.*, 2015, **6**, 8929.
32 S. Gubbala, H. B. Russell, H. Shah, B. Deb, J. Jasinski, H. Rypkema and M. K. Sunkara, *Energy Environ. Sci.*, 2009, **2**, 1302–1309.
33 K. G. Lim, H. B. Kim, J. Jeong, H. Kim, J. Y. Kim and T. W. Lee, *Adv. Mater.*, 2014, **26**, 6461–6466.
34 C. Bi, Q. Wang, Y. Shao, Y. Yuan, Z. Xiao and J. Huang, *Nat. Commun.*, 2015, **6**, 7747.
35 C. G. Wu, C. H. Chiang, Z. L. Tseng, M. K. Nazeeruddin, A. Hagfeldt and M. Grätzel, *Energy Environ. Sci.*, 2015, **8**, 2725.